HHS Public Access

Author manuscript

Nature. Author manuscript; available in PMC 2010 August 04.

Published in final edited form as:

Nature. 2010 February 4; 463(7281): 689–692. doi:10.1038/nature08722.

Structure of the Amantadine Binding Site of Influenza M2 Proton Channels In Lipid Bilayers

Sarah D. Cady[1], **Klaus Schmidt-Rohr**[1], **Jun Wang**[2], **Cinque S. Soto**[2], **William F. DeGrado**[2], and **Mei Hong**[1]

[1] Department of Chemistry, Iowa State University, Ames, IA 50011

[2] Department of Biochemistry & Biophysics, School of Medicine, and Department of Chemistry University of Pennsylvania, Philadelphia, PA 19104-6059

Abstract

The M2 protein of influenza A virus is a membrane-spanning tetrameric proton channel targeted by the antiviral drugs amantadine and rimantadine [1]. Resistance to these drugs has compromised their effectiveness against many influenza strains, including pandemic H1N1. A recent crystal structure of M2(22-46) showed electron densities attributed to a single amantadine in the N-terminal half of the pore [2], suggesting a physical occlusion mechanism for inhibition. However, a solution NMR structure of M2(18-60) showed four rimantadines bound to the C-terminal lipid-facing surface of the helices [3], suggesting an allosteric mechanism. Here we show by solid-state NMR spectroscopy that two amantadine-binding sites exist in M2 in phospholipid bilayers. The high-affinity site, occupied by a single amantadine, is located in the N-terminal channel lumen, surrounded by residues mutated in amantadine-resistant viruses. Quantification of the protein – amantadine distances resulted in a 0.3 Å-resolution structure of the high-affinity binding site. The second, low-affinity, site was observed on the C-terminal protein surface, but only when the drug reaches high concentrations in the bilayer. The orientation and dynamics of the drug are distinct in the two sites, as shown by ^{2}H NMR. These results indicate that amantadine physically occludes the M2 channel, thus paving the way for developing new antiviral drugs against influenza viruses. The study demonstrates the ability of solid-state NMR to elucidate small-molecule interactions with membrane proteins and determine high-resolution structures of their complexes.

The M2 protein of influenza A viruses is a modular, multifunctional protein that plays important roles in the acidification and uncoating of the endosome-entrapped virus and in

---

Corresponding author: Mei Hong, Tel: 515-294-3521, Fax: 515-294-0105, mhong@iastate.edu.

Supplementary information is linked to the online version of the paper at www.nature/com/nature.

Author contributions S.D.C, M.H. and K.S-R conducted SSNMR experiments. J.W. synthesized perdeuterated Amt and unlabeled M2. K.S-R carried out distance simulations. S.D.C. M.H. C.S.S. and W.F.D. analyzed the data and calculated the structure. M.H. and W.F.D. wrote the paper with inputs from other authors. M.H. designed and supervised the project.

Author information Reprints and permissions information are available at www.nature.com/reprints. One of the authors declares competing financial interest (WFD chairs the scientific advisory board of InfluMedix, a company that is working on the pharmaceutical intervention of influenza virus infections.) Correspondence and requests for materials should be addressed to M.H. (mhong@iastate.edu).

viral assembly and budding [1,4]. Its proton-conducting activity is mediated by a single transmembrane (TM) domain that forms a four-helix bundle, which acts as a pH-activated proton channel. The TM domain alone is sufficient for tetramerization [5,6] and for amantadine-sensitive proton conductivity in vesicles and cell membranes [7,8].

The recent low pH crystal structure of micelle-solubilized M2(22-46) shows a single molecule of amantadine (Amt) in the N-terminal pore lumen, consistent with the known stoichiometry of binding [8] and the location of resistant mutations, including Leu 26, Val 27, Ala 30, Ser 31, and Gly 34 [9-11]. However, the low-pH state of the protein is only transiently populated in acidifying endosomes, whereas the drug first binds with higher affinity to the protein near neutral pH [9]. Thus, determining the structure of the drug-complexed M2 protein at neutral pH is important for understanding its mechanism of inhibition. The solution NMR structure of micelle-solubilized M2(18-60) at pH 7.5 failed to show strong nuclear Overhauser effects (NOEs) between the drug and pore-lining residues, but it would have been difficult to observe NOEs between the fast-relaxing pore-lining residues and unlabeled rimantadine undergoing restricted motion in the pore. Weak NOEs were observed between residues on the protein surface and the drug, which, however, comprised 13% of the detergent in which the protein was dissolved (200-fold excess over protein tetramers). We thus turned to solid-state NMR (SSNMR), which allows for investigation of the dynamics and contacts of drug molecules bound at variable concentrations to membrane proteins in phospholipid bilayers, which are far better mimics of biological membranes than are micelles.

Rotational-echo double-resonance (REDOR) NMR is a powerful method to measure sub-nanometer inter-atomic distances with up to 0.1-Å accuracy [12]. The M2 peptide (residues 22-46), reconstituted into DMPC vesicles at pH 7.5 under fully tetrameric conditions [6,13], contained uniformly ^{13}C-labeled residues whose ^{13}C chemical shifts were assigned from 2D correlation spectra (Supplementary Fig. 1). Amantadine was perdeuterated, thus enabling ^{13}C{^{2}H} REDOR distance measurements.

To select for the highest-affinity binding site, we first measured the REDOR spectra of Amt-complexed M2 at an Amt/peptide molar ratio (Amt/P) of 1:4 (one drug per tetramer). At this stoichiometric concentration, Amt binds only to the luminal site: Fig. 1a shows ^{13}C{^{2}H} REDOR spectra without (S_0) and with (S) multiple ^{2}H dephasing pulses [14]. The Ser31 Cα signal is strongly dephased by the deuterons (S/S_0 = 0.76 ± 0.03 at 10.1 ms), indicating that Amt binds near Ser 31. In contrast, the Asp44 Cα signal in the peripheral site is unaffected. A double-quantum-filtered REDOR experiment that removed all lipid signals confirmed the lack of Asp 44 dephasing (Supplementary Fig. 2).

To search for additional, lower-affinity, binding sites, we increased the Amt concentration to Amt/P = 4 : 4, making the drug 7% of the amphiphiles composing the bilayer, which approaches the large excess of drug in the solution NMR experiments. Now the Asp44 Cα signal is also dephased (S/S_0 = 0.86 ± 0.02 at 10.1 ms), but to a lesser extent than Ser31 Cα (Fig. 1b). Thus, when free amantadine is a major component of the membrane, Amt contacts the C-terminus of the protein as in the solution NMR structure, [3] but without displacing the drug in the luminal site. Consistently, Amt deuterons also dephased other residues in the

luminal site, particularly Val27 Cγ1 and Gly34 Cα (Fig. 1c, d), but more weakly than Ser 31. This Ser 31-proximal binding is consistent with the large chemical shift perturbation of Ser 31 by Amt [15].

^{2}H NMR provided exquisite details on the orientation and dynamics of amantadine, whose unique symmetry and rigidity simplify analysis. Amantadine is a rigid amphiphile with a polar amine and a hydrophobic adamantane centered around a 3-fold axis, Z_M. Three axial C-D bonds are parallel to Z_M while twelve equatorial C-D bonds are at 70° or 110° (θ_{PM}) from Z_M (Fig. 2d). Amantadine partitions strongly into protein-free DMPC vesicles and exhibit ^{2}H quadrupolar splittings of 36 and 123 kHz with a 4:1 intensity ratio at 243 K (Fig. 2a). These splittings indicate fast anisotropic rotation of the molecule around Z_M, which scales the couplings from the rigid-limit value of 125 kHz by $(3cos^2\theta_{PM}-1)/2$, giving 40 kHz for the twelve equatorial bonds and 125 kHz for the three axial bonds. Wobbling of the Z_M axis by ∼6° likely accounts for the additional motional averaging. As the temperature increased to 303 K, the couplings decreased twofold (18 and 58 kHz) while maintaining the same 1:3 frequency ratio and 4:1 intensity ratio. The ±0.46 scaling factor indicates Amt rotates rapidly around the normal ($\vec{n}$) of the liquid-crystalline bilayer in addition to its own axis, with Z_M tilted by 37° or 80° from $\vec{n}$ (Fig. 2e) [16].

When a stoichiometric amount (Amt/P = 1 : 4) of protein is present, the Amt spectrum at 243 K resembles the lipid-only spectrum, but the couplings remain unchanged from 243 to 303 K across the membrane phase transition (Fig. 2b), indicating sequestration of the drug from the lipids. The constant scaling factor (0.93) compared to pure rotation around Z_M indicates that the first equivalent of Amt rotates rapidly around $\vec{n}$ in a slightly tilted orientation (∼13°) between Z_M and $\vec{n}$ (Fig. 2d). An isotropic peak grows at high temperature, indicating a small fraction (∼12% at 303 K) of Amt either near 54.7° from the membrane normal or undergoing large-angle tumbling in the channel. Finally, a weak 18-kHz splitting is observed at 303 K that matches the lipid-only coupling at this temperature. The spectrum is consistent with a 9:1 combination of the 283 K M2-bound spectrum without the 18-kHz splitting and the 303 K lipid-bound spectrum, suggesting that 10% of the drug partitions into the bilayer at 303 K.

To confirm that the lumen-bound drug persists under drug excess and to probe for additional binding sites, we measured the ^{2}H spectra under 4-fold excess Amt over the tetramer (corresponding to 12% of the lipid concentration). Fig. 2c shows that the spectroscopic signatures of the lumen-bound drug persists, but the 303 K spectrum is now the 1:3 combination of the stoichiometric spectrum (Fig. 2b) and the lipid-bound spectrum (Fig. 2a). No additional bound species was detected. Since the 4-fold symmetry of the channel requires four peripheral sites for each luminal site, the 9:1 intensity ratio of the 303 K stoichiometric spectrum suggests that Amt has at least a 40-fold greater affinity for the channel lumen than the peripheral site.

These ^{2}H NMR and distance data indicate that M2 has a single high-affinity site for amantadine, located in the channel lumen centered at Ser 31. In this site, Amt is nearly aligned with the channel axis, but given sufficient thermal energy a small fraction of drug is also able to undergo nearly isotropic motion, as suggested by molecular dynamics

simulations [17,18]. Excess Amt adopts a significantly tilted orientation in the membrane, with or without the protein. The peripherally bound rimantadines in the solution NMR structure are tilted by 80° [3], precisely one of the two possible orientations found for the lipid-associated drug. Since the same peripheral site is detected here in the TM peptide, its existence is independent of the protein length or the membrane environment; it is the result of excess drugs in the micelles and lipid bilayers.

To determine the sub-angstrom resolution structure of the high-affinity binding site, we quantified the M2-Amt distances using an alternative REDOR experiment containing multiple ^{13}C pulses and one ^{2}H pulse, thus minimizing ^{2}H pulse imperfections and yielding REDOR intensities closely following the universal curve [19] (Supplementary Fig. 3). The experiment yielded significantly faster REDOR dephasing (Fig. 3) while confirming the relative dephasing of different sites in Fig. 1.

Due to the 4-fold symmetry of the tetramer, we parameterized the REDOR simulations in terms of the distance R of each peptide carbon from the channel axis and the distance Z of each carbon plane from the Amt center (Fig. 3c). We considered the twelve deuterons in the two equatorial planes with rotational averaging and neglected the three axial deuterons due to poor inversion of their broad ^{2}H spectra. A series of REDOR curves were calculated for R of 2.7–6.2 Å and various Z values for each R, capturing the geometry of previous M2 structural models, (Fig. 3d-f). The curves are quite sensitive to geometry. The Ser31 Cα pore radius is most tightly constrained, to 5.7–6.3 Å. Larger R would not give sufficient dephasing even when $Z = 0$ while smaller R would shift the drug up or down the channel too much to comply with the observed intensities of Val27 Cγ1 and Gly34 Cα. The best-fit Z places Ser31 Cα in the middle of the two planes of deuterons.

We computed an ensemble of structures using these protein-drug distances and previous SSNMR constraints. The structures cluster tightly with a heavy-atom root-mean-square deviation (RMSD) of 0.3 Å (Fig. 4). The four helices are kinked at Gly 34, with the helical axis tilted by 30° for the N-terminal segment and 19° for the C-terminal segment, consistent with ^{15}N SSNMR orientational constraints [20]. The narrowest points of the pore lie at the N-terminal Val 27 and C-terminal His 37/Trp 41, which are responsible for pH sensing and proton conduction [21]. Amantadine fits snugly into the N-terminal lumen, surrounded by residues whose mutation confers resistance [9]. The surrounding backbone amides and Ser31 hydroxyl group engage in intra-helical hydrogen bonding, imparting a hydrophobic character to the site. The luminal binding indicates that M2 inhibition is by physical occlusion, interrupting water-wires and perturbing the protonation equilibrium of His37 [22]. The N-terminal location is consistent with the fact that Amt inhibits only when added to M2-expressing cells from the outward-facing N-terminal side [9]. Moreover, the V27 vestibule is too small to permit drug dissociation without a 1–2 Å radial expansion, consistent with the very slow association and dissociation of the drug compared to a diffusion-controlled process [9]. Finally, the drug is most likely oriented with the adamantane packed against the hydrophobic Val27 sidechains and the polar amine towards the cavity near His 37 residues, whose pK_a's are affected by Amt binding [22].

The present SSNMR structure has significant differences from previous proposed structures of the Amt-M2 complex [2,3]. While the drug location is very similar to that of the low-pH crystal structure, the shape of the binding site differs dramatically (3.4-Å Cα RMSD between the structures). In the crystal structure, the helices splay far apart near the C-terminus (Fig. 5b), to minimize electrostatic repulsions among the protonated His 37. In the high-pH SSNMR structure, the helices close off the bottom of the site, fully sequestering the drug and explaining the improved affinity at higher pH (Fig. 5a). The backbone of the SSNMR structure is more similar to the high-pH solution NMR structure, with comparable distances involving Val27 Cγ1, Ser31 Cα, and Gly34 Cα (Supplementary Fig. S5). Thus, the drug may have been present in the lumen in the solution NMR sample but not observable without isotopic labeling. Alternatively it might have been truly absent from the lumen due to reduced affinity to the micelle-bound and structurally plastic protein [23-25]. The current high-resolution structure also revises an earlier SSNMR chemical-shift-constrained M2 model, where the lack of protein-drug distances resulted in a large N-terminal vestibule, which would yield a highly solvent-accessible low-affinity drug (Supplementary Fig. S6-S7).

What is the significance of the peripheral site? Since it is occupied only at drug/lipid or drug/detergent ratios above 7 mol%, the protein-drug interactions at this site must be weak, and largely a consequence of the high local concentration and preference of the drug for the membrane-water interface [16]. The peripheral site may in some way be related to the partial inhibition of M2 by polyamines in the absence of sodium ions [26].

Since amantadine undergoes significant motion in the N-terminal lumen, its structure appears to be not fully optimized to fit the M2 channel. Thus, other drugs may be designed to access the most conserved regions of the pore and evade drug resistance. Indeed, a potent and structurally distinct class of inhibitors has been recently reported that binds the same site [27]. Solid-state NMR spectroscopy, especially the multi-deuteron ^{13}C-^{2}H distance strategy, opens a new avenue for structure elucidation of drug-complexed membrane proteins in lipid bilayers, yielding distances with longer range and higher accuracy than NOE measurements in solution.

Methods Summary

The ^{13}C-labeled wild-type Udorn M2(22-46) peptide was synthesized by solid-phase methods and reconstituted into DMPC bilayers at pH 7.5 by detergent dialysis [25], giving fully tetramerized protein in the liposomes [6]. $^{13}C\{^{2}H\}$ REDOR experiments were conducted on a 9.4-Tesla wide-bore NMR spectrometer (Bruker Biospin) using a 4 mm $^{1}H/^{13}C/^{2}H$ MAS probe. The distances were measured at 243 K, where the peptide was immobilized [28] while Amt was uniaxially mobile. Static ^{2}H spectra were measured on a 14.1-Tesla SSNMR spectrometer.

An ensemble of 17 lowest-energy SSNMR structures was computed using 24 (6×4) long-range ^{13}C-^{2}H distances, four inter-helical distances among Trp41 indole rings [13], 60 (15×4) backbone amide orientational constraints [20], two sidechain rotamer constraints [29], and idealized covalent geometry. For comparison, the previous solution NMR M2 structure

ensemble was constrained by 12 inter-helical NOEs and 18 amide residual dipolar couplings for the TM region [3]. The structure ensemble has been deposited in the Protein Databank (ID: 2KQT) and the BMRB (ID: 16612).

Methods

Sample preparation

The wild-type Udorn M2(22-46) sequence SSDPLVVAASIIGILHLILWILDRL was synthesized with ^{13}C, ^{15}N-labeled amino acids at Leu 26, Val 27, Ala 29 and Gly 34 in one sample (LVAG), and Ser 31, Ile 32, and Asp 44 in another sample (SID). The peptide was reconstituted into DMPC vesicles by detergent dialysis using octyl-β-D-glucopyranoside. The peptide/lipid molar ratios were 1:8 for all ^{2}H NMR experiments and 1:8 or 1:15 for the REDOR experiments. A phosphate buffer (pH 7.5) was used for lipid vesicle preparation and throughout detergent dialysis. The dialyzed proteoliposome solutions were centrifuged at 150,000 g to obtain ∼40% hydrated membrane pellets. Amantadine was directly titrated into the membrane pellet to the desired amount.

Solid-state NMR spectroscopy

A triple-resonance $^{1}H/^{13}C/^{2}H$ magic-angle-spinning (MAS) probe was used for the ^{13}C-^{2}H REDOR experiments and a $^{1}H/^{13}C/^{15}N$ probe was used for 2D correlation experiments for resonance assignment. The ^{2}H pulse length in the REDOR experiments was 6.2 μs, and ^{13}C and ^{15}N pulse lengths were 5-6 μs.

^{13}C-^{2}H REDOR experiments were carried out at MAS frequencies of 4250 Hz or 4750 Hz. A REDOR pulse sequence containing a single selective ^{13}C pulse and multiple composite ^{2}H pulses was used to obtain clear qualitative dephasing at long mixing times, since the selective ^{13}C pulse suppressed the ^{13}C-^{13}C scalar coupling and gave rise to long ^{13}C T_2 relaxation times. However, the use of multiple ^{2}H pulses is known to slow down dipolar dephasing by the cumulative effects of imperfect inversion of the broad ^{2}H quadrupolar spectra [30]. Thus, a second version of REDOR experiment consisting of multiple ^{13}C non-selective pulses and a single composite ^{2}H pulse was carried out to obtain quantitative dephasing values at shorter mixing times. Distance quantification was possible because the multiple heteronuclear couplings commute and the uniaxial rotation of amantadine removes the effects of ^{2}H-^{2}H homonuclear couplings. Perdeuteration speeded up ^{13}C-^{2}H REDOR dephasing by $\sim \sqrt{15}$-fold compared to a single ^{13}C-^{2}H pair. The inversion efficiency of the deuterons in the single-^{2}H-pulse REDOR experiment was 70% based on measurements of the model compound $^{13}C\alpha$, $^{2}H\beta$-labeled alanine (Supplementary Fig. 3).

REDOR distance simulations

Using a motionally averaged model, we calculated REDOR curves for various published M2 models (Supplementary Fig. S4-6), with pore radii R of 2.7 – 6.2 Å. For each R, several REDOR curves with different Z values were calculated. The best-fit Z values for a specific R were compared with the carbon plane separations in the structural model. Plane separations that are inconsistent with the differences in Z values exclude the structural

model. The Ser31 Cα pore radius is constrained by the M2-drug distances to be 5.7 – 6.3 Å. Once amantadine is confined within 1 Å vertical distance of the Ser31 Cα plane, the Val27 Cγ1 and Gly34 Cα pore radii are jointly constrained by the Val27 Cγ1 – Gly34 Cα plane separation, which is 10.5 ± 1.0 Å in all M2 structures so far. We found that neither R_V nor R_G can exceed 6.0 Å, as it would lead to overly small plane separations.

In the final refined SSNMR structure, Val27 Cγ1 is fit by $R_V = 3.8$ *Å* with $Z_V = -5.3$ Å, indicating that the Val27 Cγ1 plane is 5.3 Å above the center of amantadine. Gly34 Cα is fit by $R_G = 4.9$ *Å* with a distance of 5.0 Å below the amantadine center.

Structure calculation and refinement

The process of generating a helix that is consistent with the protein-drug distances, backbone N-H orientational constraints, and sidechain rotameric conformations, was carried out in two phases. In the first phase, we constructed an ideal helix with the sequence SSDPLVVAASIIGILHLILWILDRL whose φ/ψ angles were set to (-65°, -42°). The helix was then split at the Gly34-Ile35 bond and reconnected using a rigid-body optimization procedure that maximized agreement with the SSNMR ^{15}N-^{1}H dipolar couplings [20] and the internal geometry at that bond. Rotamer preferences were taken from the high-resolution X-ray structure of M2 (PDB ID: 3BKD).

In the second phase we refined our model to maximize agreement with the ^{13}C-^{2}H REDOR distances (Supplementary Table S2) and the backbone ^{15}N-^{1}H dipolar couplings (Supplementary Table S3). To do this, we combined an inverse kinematics algorithm with a Monte Carlo/Simulated Annealing (MC/SA) minimization procedure that would gradually relax the backbone of the helix subject to REDOR distance constraints and the N-H dipolar couplings. Rotamer preferences were also changed to maximize agreement with the χ_1 angle constraints (Supplementary Table S4). The MC/SA minimization procedure was used to generate an ensemble with a maximum heavy-atom RMSD of 0.3 Å between any two models. Since the REDOR distances provided excellent constraints between the drug and M2, we positioned the amantadine molecule near Ser 31 without the need for further minimization. Fig. 5 was created using the PyMOL Molecular Graphics System.

Supplementary Material

Refer to Web version on PubMed Central for supplementary material.

Acknowledgments

This work was supported by a NSF grant MCB-0543473 and an NIH grant GM088204 to M.H., the Iowa State University Foundation, and NIH grants GM56423 and AI74571 to W.F.D.

References

1. Cady SD, Luo WB, Hu F, Hong M. Structure and function of the influenza M2 proton channel. Biochemistry. 2009; 48:7356–7364. [PubMed: 19601584]
2. Stouffer AL, et al. Structural basis for the function and inhibition of an influenza virus proton channel. Nature. 2008; 451:596–599. [PubMed: 18235504]

3. Schnell JR, Chou JJ. Structure and mechanism of the M2 proton channel of influenza A virus. Nature. 2008; 451:591–595. [PubMed: 18235503]

4. Pinto LH, Lamb RA. The M2 Proton Channels of Influenza A and B Viruses. J Biol Chem. 2006; 281:8997–9000. [PubMed: 16407184]

5. Salom D, Hill BR, Lear JD, DeGrado W. F pH-dependent tetramerization and amantadine binding of the transmembrane helix of M2 from the influenza A virus. Biochemistry. 2000; 39:14160–14170. [PubMed: 11087364]

6. Luo W, Hong M. Determination of the oligomeric number and intermolecular distances of membrane protein assemblies by anisotropic 1H-driven spin diffusion NMR spectroscopy. J Am Chem Soc. 2006; 128:7242–7251. [PubMed: 16734478]

7. Stouffer AL, et al. The interplay of functional tuning, drug resistance, and thermodynamic stability in the evolution of the M2 proton channel from the influenza A virus. Structure. 2008; 16:1067–1076. [PubMed: 18611380]

8. Ma C, et al. Identification of the Functional Core of the Influenza A Virus A/M2 Proton-Selective Ion Channel. Proc Natl Acad Sci USA. 2009; 106:12283–12288. [PubMed: 19590009]

9. Wang C, Takeuchi K, Pinto LH, Lamb RA. Ion channel activity of influenza A virus M2 protein: characterization of the amantadine block. J Virol. 1993; 67:5585–5594. [PubMed: 7688826]

10. Jing X, et al. Functional studies indicate amantadine binds to the pore of the influenza A virus M2 proton-selective ion channel. Proc Natl Acad Sci USA. 2008; 105:10967–10972. [PubMed: 18669647]

11. Holsinger LJ, Nichani D, Pinto LH, Lamb RA. Influenza A virus M2 ion channel protein: a structure-function analysis. J Virol. 1994; 68:1551–1563. [PubMed: 7508997]

12. Gullion T, Schaefer J. Rotational echo double resonance NMR. J Magn Reson. 1989; 81:196–200.

13. Luo W, Mani R, Hong M. Sidechain conformation and gating of the M2 transmembrane peptide proton channel of influenza A virus from solid-state NMR. J Phys Chem. 2007; 111:10825–10832.

14. Jaroniec CP, Tounge BA, Herzfeld J, Griffin RG. Frequency Selective Heteronuclear Dipolar Recoupling in Rotating Solids: Accurate 13C-15N Distance Measurements in Uniformly 13C, 15N-labeled Peptides. J Am Chem Soc. 2001; 123:3507–3519. [PubMed: 11472123]

15. Cady SD, Mishanina TV, Hong M. Structure of amantadine-bound M2 transmembrane peptide of influenza A in lipid bilayers from magic-angle-spinning solid-state NMR: the role of Ser31 in amantadine binding. J Mol Biol. 2009; 385:1127–1141. [PubMed: 19061899]

16. Li C, Yi M, Hu J, Zhou HX, Cross TA. Solid-state NMR and MD simulations of the antiviral drug amantadine solubilized in DMPC bilayers. Biophys J. 2008; 94:1295–1302. [PubMed: 17890391]

17. Yi M, Cross TA, Zhou HX. A secondary gate as a mechanism for inhibition of the M2 proton channel by amantadine. J Phys Chem B. 2008; 112:7977–7979. [PubMed: 18476738]

18. Chen H, Wu Y, Voth GA. Proton transport behavior through the influenza A M2 channel: insights from molecular simulation. Biophys J. 2007; 93:3470–3479. [PubMed: 17693473]

19. Gullion T. Measuring 13C–2D Dipolar Couplings with a Universal REDOR Dephasing Curve. J Magn Reson. 1999; 146:220–222. [PubMed: 10968975]

20. Hu J, et al. Backbone stucture of the amantadine-blocked transMembrane domain M2 proton channel from influenza A virus. Biophys J. 2007; 92:4335–4343. [PubMed: 17384070]

21. Tang Y, Zaitseva F, Lamb RA, Pinto LH. The Gate of the Influenza Virus M2 Proton Channel Is Formed by a Single Tryptophan Residue. J Biol Chem. 2002; 277:39880–39886. [PubMed: 12183461]

22. Hu J, Riqiang F, Cross TA. The Chemical and Dynamical Influence of the Anti-Viral Drug Amantadine on the M2 Proton Channel Transmembrane Domain. Biophys J. 2007; 93:276–283. [PubMed: 17434944]

23. Cristian L, Lear JD, DeGrado WF. Use of thiol-disulfide equilibria to measure the energetics of assembly of transmembrane helices in phospholipid bilayers. Proc Natl Acad Sci USA. 2003; 100:14772–14777. [PubMed: 14657351]

24. Li C, Qin H, Gao FP, Cross TA. Solid-state NMR characterization of conformational plasticity within the transmembrane domain of the influenza A M2 proton channel. Biochim Biophys Acta. 2007; 1768:3162–3170. [PubMed: 17936720]

25. Cady SD, Hong M. Amantadine-Induced Conformational and Dynamical Changes of the Influenza M2 Transmembrane Proton Channel. Proc Natl Acad Sci USA. 2008; 105:1483–1488. [PubMed: 18230730]
26. Lin TI, Heider H, Schroeder C. Different modes of inhibition by adamantane amine derivatives and natural polyamines of the functionally reconstituted influenza virus M2 proton channel protein. J Gen Virol. 1997; 78:767–774. [PubMed: 9129648]
27. Wang J, et al. Discovery of spiro-piperidine inhibitors and their modulation of the dynamics of the M2 proton channel from influenza A virus. J Am Chem Soc. 2009; 131:8066–8076. [PubMed: 19469531]
28. Luo W, Cady SD, Hong M. Immobilization of the Influenza A M2 Transmembrane Peptide in Virus-Envelope Mimetic Lipid Membranes: A Solid-State NMR Investigation. Biochemistry. 2009; 48:6361–6368. [PubMed: 19489611]
29. Hong M, Mishanina TV, Cady SD. Accurate measurement of methyl 13C chemical shifts by solid-state NMR for the determination of protein sidechain conformation: the influenza M2 transmembrane peptide as an example. J Am Chem Soc. 2009; 131:7806–7816. [PubMed: 19441789]
30. Sack I, Goldbourt A, Vega S, Buntkowsky G. Deuterium REDOR: Principles and applications for distance measurements. J Magn Reson. 1999; 138:54–65. [PubMed: 10329226]

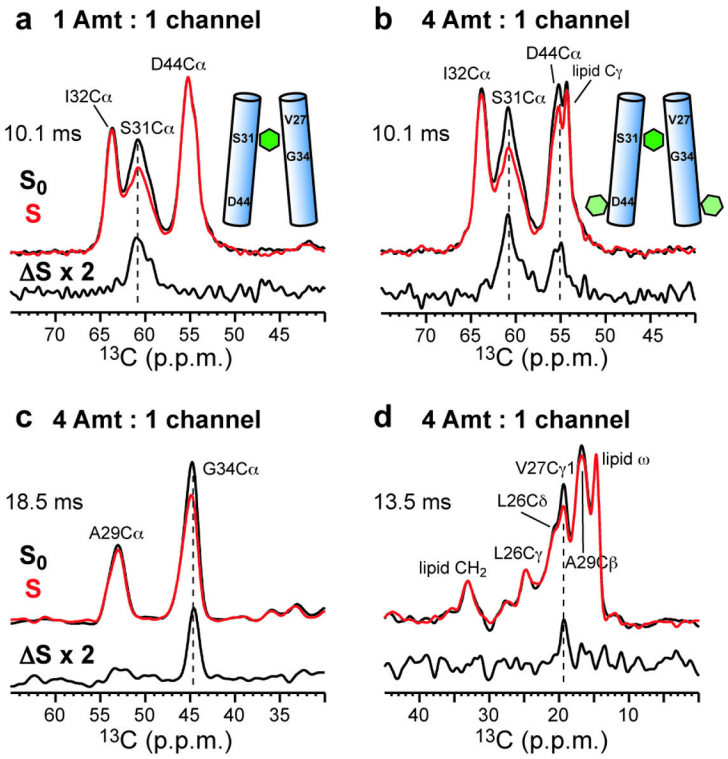

Figure 1. Drug-protein proximities from $^{13}C\{^{2}H\}$ REDOR spectra of Amt-bound M2 in DMPC bilayers at two Amt/P ratios

Control (S_0), dephased (S, red), and difference (ΔS) spectra at specified mixing times are shown. **a.** Ser31, Ile32, Asp44-labeled (SID) M2 at the stoichiometric ratio of Amt/P = 1 : 4. **b.** SID-M2 at the 4-fold excess ratio of Amt/P = 4 : 4. Ser31 Cα is dephased under both conditions but Asp44 Cα is dephased only when Amt is in excess. **c-d.** Leu26, Val27, Ala29, and Gly34-labeled (LVAG) M2 at Amt/P = 4 : 4. **c.** Gly34 Cα region. **d.** Val27 Cγ1 region.

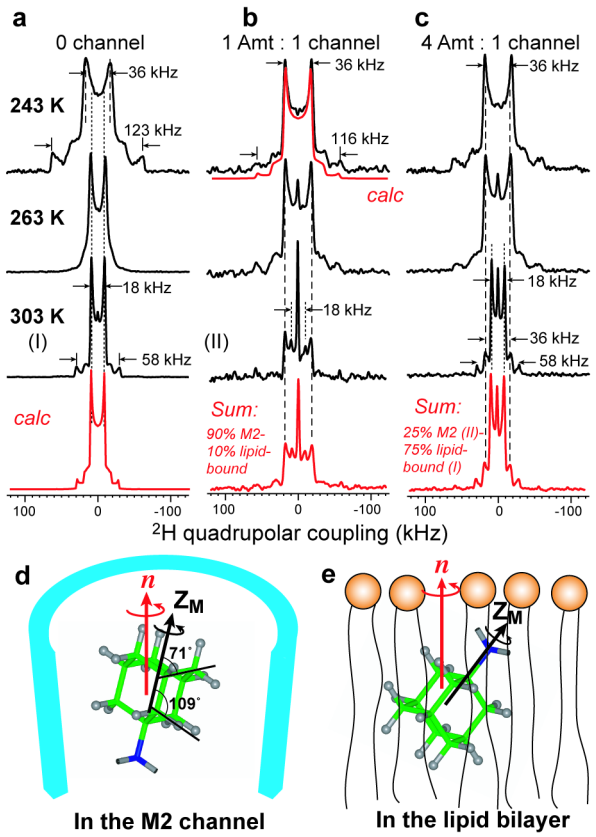

Figure 2. ^{2}H NMR spectra of d_{15}-Amt in DMPC bilayers as a function of temperature and Amt/P

a. No M2. The calculated spectrum for 303 K reproduces the 1:3 frequency ratio and 4:1 intensity ratio of the two splittings. **b** Amt/P = 1: 4. The sum spectrum reproduces the 303 K spectrum by 1:9 combination of the lipid-bound 303 K spectrum and peptide-bound 283 K spectrum (not shown). **c.** Amt/P = 4 : 4. The sum spectrum uses a 1:3 combination of the M2-bound spectrum (II) and lipid-bound spectrum (I). **d.** Amt orientation in the M2 channel. **e.** One of the two possible Amt orientations in the lipid bilayer.

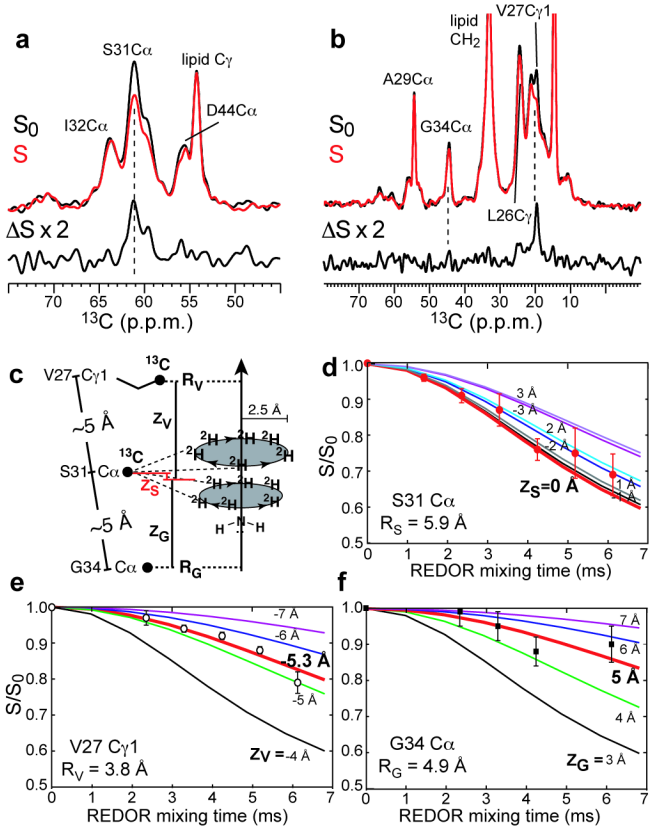

Figure 3. M2-Amt distance quantification

a-b. $^{13}C\{^{2}H\}$ REDOR spectra of Amt-bound M2 (Amt/P = 4 : 4) obtained by the single-^{2}H-pulse REDOR. **a.** SID-M2 at 4.2 ms mixing. **b.** LVAG-M2 at 6.1 ms mixing. **c-f.** REDOR simulations. **c.** Definition of the pore radius R and height difference Z from the center of Amt. **d.** Ser31 Cα simulation. **e.** Val27 Cγ1 simulation. **f.** Gly34 Cα simulation.

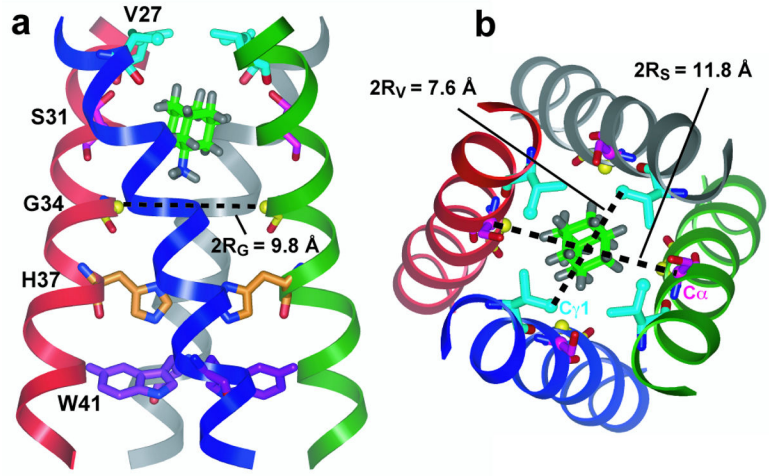

Figure 4. SSNMR structure of Amt-bound M2 in lipid bilayers

a. Side view showing Ser 31, Val 27, Gly 34, His 37, Trp 41, and Amt in the high-affinity luminal site. Ser31 Cα lies in the mid-plane between the two rings of deuterons. The instantaneous orientation of Amt, which is slightly tilted from the channel axis, is shown. The time-averaged Amt orientation is parallel to the channel axis. **b** Top view showing the Ser 31 and Val 27 pore radii. This ribbon diagram was generated using the program Insight II.

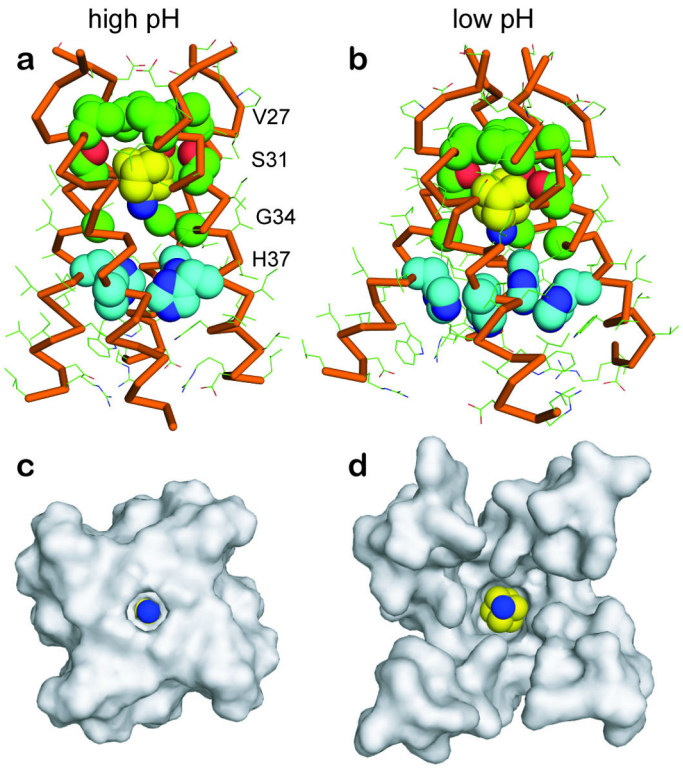

Figure 5. Comparison of the high-pH SSNMR structure of Amt-bound M2 in lipid bilayers with the low-pH crystal structure of Amt-bound M2

a. Side view of the high-pH SSNMR structure, showing Amt to be enclosed by Val 27 at the top and His 37 at the bottom. **b.** Side view of the low-pH crystal structure [2]. The helices are splayed far apart near the C-terminus. **c.** C-terminal view of the high-pH structure, showing a well-sequestered drug. **d.** C-terminal view of the low-pH structure, showing a more solvent-accessible drug. The figure was generated using the program PyMOL.